PHASE PLANE ANALYSIS AND OBSERVED FROZEN ORBIT FOR THE TOPEX/POSEIDON MISSION

Bruce E. Shapiro

Jet Propulsion Laboratory
California Institute of Technology
Pasadena, California

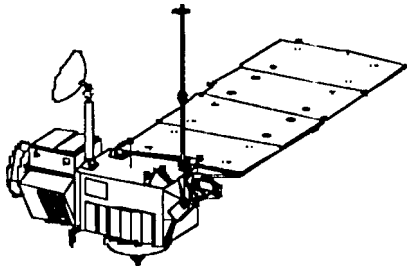

Sixth International Space Conference of Pacific Basin Societies

◆ American Astronautical Society ◆ Japanese Rocket Socicty ◆ Chinese Society of Astronautics ●

"Strengthening Cooperation in the 21st Century"

MARINA DEL REY, CALIFORNIA, USA 6-8 DECEMBER 1995

AAS Publications Office, P.O. Box 28130, San Diego, CA 92198

PHASE PLANE ANALYSIS AND OBSERVED FROZEN ORBIT FOR THE TOPEX/POSEIDON MISSION*†

Bruce E. Shapiro**

The existence and stability of low eccentricity frozen orbits in a zonal geopotential perturbed by atmospheric drag, solar radiation pressure (SRP), and a continuous along-track thrust is studied. General expressions are derived for the steady state eccentricity and gravity-only phase plane trajectories. These gravity-only counters are limit cycles that arise from a Hopf bifurcation as non-gravitational perturbations pass through zero. Drag is stabilizing and thrust may be either stabilizing or non-stabilizing. A saddle/node bifurcation is introduced by SRP. Variations due to shadowing and solar geometry cause the steady state to significantly depart from its unperturbed value. This leads to a complicated phase portrait which can fold back on itself as the bifurcation parameters change dynamically. While the TOPEX/Poseidon geometry is such that the saddle/node bifurcation is not crossed if can be crossed repeatedly in other satellite configurations. The TOPEX/Poseidon satellite has remained in a frozen orbit throughout its three year primary mission and is expected to remain so during the extended mission without any eccentricity maintenance maneuvers being required. Orbital data are used to illustrate the abstract models.

INTRODUCTION

Earth observation missions such as TOPEX/Poseidon are frequently placed in low eccentricity frozen orbits with the perigee fixed at 90". In such an orbit, the mean argument of perigee, ω, and mean eccentricity, e, arc kept in the neighborhood of a stable critical point. Deviations from the critical point lead to closed curves in the (e,ω) phase plane when only central-body gravitational perturbations are considered. These trajectories remain in the neighborhood of the critical point even under the influence of such perturbing forces as drag and solar radiation pressure (SRP). Orbital maneuvers can be applied to recover any significant errors which may accumulate. Frozen orbits exist at all inclinations, even though they arc frequent.fy thought to exist only for nearly-cirmlar nearly-polar and nearly-equatorial orbits and at high eccentricity near the critical inclination (e.g. Molniya orbits), they exist at all inclinations. The low-eccentricity frozen orbit was first described for SEASAT' but has also been studied for numerous other earth-orbiting missions, including the Atmospheric Explorer,[2,3] the Heat Capacity Mapping Mission,[2,3] LANDSAT,[4] GEOSAT,[5-8] and TOPEX/Poseidon,[9,10] as well as for Martian,[11,12] Venusian,[13] and Lunar[14] orbiters. In a more general sense, the expression *frozen orbit can also* refer to geo-synchronous and sun-synchronous orbits.[15]

Existence of the frozen orbit is usually attributed to the balancing of the secular perturbations of the even zonal harmonics with the long period perturbations of the odd zonal harmonics.[16] Early treatments obtained an analytic solution through J3 which was then extended to higher degree zonals via numerical integration of the mean elements.[1-3,5,9,10] From a more abstract perspective, frozen orbits arise from bifurcations[17,18] or singularities[12] in the relevant system of differential equations obtained via the appropriate Hamiltonian or Lagrangian formulation. While cam must be taken to ensure that the definition of mean elements is compatible with the dynamic formulation, the approach taken is largely a function of individual authors' personal biases toward the problem being studied.

Bifurcations arise when constants in the dynamic equations are treated as parameters and allowed to vary over some physically (or mathematically) realizable range. If the flows of the dynamic system become

---

' Presented at the Sixth International Space Conference of Pacific Basin Societies, Marina del Rey, CA, 6-6 December 19%.

The research this paper was carried cut by the Jet Propulsion Laboratory, California Institute of Technology, ' under contract with the National Aeronautics and Specs Administration.

** Member, Technical Staff, Jet Propulsion Laboratory, 4800 Oak Grove Drive, Pasadena, CA, 91109. Electronic mail: Bruce. E. Shapiro@jpl.nasa.gov.

structurally unstable for some values of these parameters -- i.e. the phase portraits of the original and ε-perturbed systems of differential equations are not topologically equivalent --a *bifurcation* is said to occur.[19] Besides being interesting from an abstract point of view, bifurcations have pragmatic significance: at bifurcation points, the nature and stability of the critical points may change. This allows the mission design engineer to identify and classify bread classes of orbits and their sensitivity to various types of perturbations without the usual black-box approach of tedious numerical integrations. *Hopf bifurcations* form a particularly interesting class of bifurcations. This is because of the theorem, first proven by Hopf in 1942, that proves the existence of stable limit cycles (e.g., closed orbits) in the neighborhood of a Hopf bifurcation, under certain conditions. A Hopf bifurcation can be identified as follows. Suppose that the eigenvalues of the Jacobian form a complex conjugate pair $\lambda = a \pm ib$. A Hopf bifurcation occurs if $\mathrm{Re}\,\lambda$ passes through O with $\mathrm{Im}\,\lambda \neq 0$ as some parameter of the system is varied.

The theory of bifurcations can be used to *define* a specific mission's frozen orbit in terms of its existence and stability properties under quiescent conditions (e.g., low solar and geomagnetic activity). The process begins with a two-body Hamiltonian for the earth/satellite gravitational interaction. Perturbations are added as zonal harmonics describing the Earth's oblateness. As these zonals are added, a tapestry of bifurcations slowly unfolds. Three families of frozen orbits have been identified in this manner: (1) stable and (2) unstable families arising from Hopf bifurcations at the critical inclination, and (3) a stable family starting in the equatorial plane.[15] A member of one of these families is then selected as the mission orbit, Non-gravitational perturbing forces such as drag, thrust, or solar radiation pressure are then added to the equations of motion. If the subsequently perturbed orbit remains frozen and within mission specifications, all is well. If not, further examination of the stability of the perturbed orbit can be performed to determine the extent of maneuvering which will be necessary to maintain some approximation of a frozen orbit. There is the added complication that the usual perturbations of interest are non-conservative functions of extremely dynamic variables (e.g. solar flux, atmospheric density, satellite attitude) and the resulting system of equations becomes non-autonomous.

In the present analysis the Lagrangian formulation is utilized and phase space is reduced to two dimensions by assuming that the inclination and semi-major axis are constant. While this simplification is appealing since it permits the application of such results as the *Hartman-Grobman theorem* (that the flows of the nonlinear system, *in two dimensions, are* homomorphic to the linear system in some neighborhood of the steady state), it is also physically reasonable if a and i can be kept fixed via orbitat maneuvers" independently of e and ω. A general solution for the frozen eccentricity is then derived. The stability of this solution is examined in the phase plane under the influence of various perturbing forces. It is shown that the frozen orbit arises out of a Hopf bifurcation when non-gravitational forces disappear; limit cycles appear in the neighborhood of the steady state when the perturbations are small. Drag is stabilizing, while thrust can be either stabilizing or destabilizing. Solar radiation pressure has a complicated parameter space describing the orbital/solar geometry which is continually changing. This causes the steady state to depart significantly from the unperturbed state, thereby dragging the phase plane trajectories with it. For some satellite/orbital configurations, the steady state can cross additional saddle-node bifurcations as the sun moves through its β' cycle. This allows the (e,ω) trajectory to double back upon itself and curlicue through the phase plane, a situation which would not be possible in the case of fixed perturbations.

Numerical examples and observations of the TC)PEX/Poseidon satellite frozen orbit taken during its primary thrco-year mission arc provided. This joint US/French mission*" studies global ocean circulation and its interaction with the atmosphere to better understand the Earth's climate. This goal is accomplished utilizing a combination of satellite altimetry data and orbit determination to precisely determine ocean surface topography. The satellite is maintained in a nearly circular, frozen orbit ($e \approx 95$ PPM† and $\omega \approx 90°$) at an altitude of ≈1336 km and an inclination of $i \approx 66.04°$. This orbit provides an

---

" In fact, in the absence of dra and solar radiation pressure, there are no bng term or secular perturbation on a, while the long-term variation in inclination due to centre-body gravity is smaller by a factor of e than the variation of e itself.

." The TOPEX/Poseidon Mission is jointly funded b ive US National Aeronautic and Space Administration (NASA) and the French *Centre National d'Etudes Spatiales (CNES).*

† Parts per million. The difference between the value quoted hem and the value derived in the following section is due to the selection of the operational orbit based upon early numerical calculations which truncated the zonal expansion atJ17.

exact repeat ground track every 127 revolutions (≈9.9 days) and overflies two altimeter verification sites. TOPEX/Poseidon was launched by an Ariane 42P on August 10, 1992. The operational orbit was acquired some 42 days later, on September 21, 1992, following a sequence of six maneuvers.[m]

STEADY STATE SOLUTIONS

The relevant system of differential equations can be obtained from Merson's[21] implementation of GrOVCS'22 formulation (see equations A20 and A32 in the appendix). Omitting the explicit dependence upon semi-major axis and inclination,

$$\frac{d\omega}{dt} = B(a,i) + [(1/e)G(a,i) - eD(a,i)]\sin\omega \qquad (1)$$

$$\frac{de}{dt} = -G(a,i)\cos\omega \qquad (2)$$

where *B, D,* and G arc given by equations A29, A35, and A31. From equation 2 steady state solutions (corresponding to $\dot{e} = \dot{\omega} = 0$) are possible at either the orbital "north pole" ($\omega = 90°$) or the orbital "south pole" ($\omega = 270°$). It will be seen that only onc of these solutions is possible for any given combination of inclination and semi-major axis. Furthermore, although equation 1 produces a quadratic for the steady state eccentricity, there will be a unique physically realizable solution. At the orbital north pole,

$$-De^2 + Be + G = 0 \qquad (3)$$

and hence

$$e = \frac{-B \pm \sqrt{B^2 + 4DG}}{-2D} \qquad (4)$$

Only onc of these solutions will produce a physically realizable solution ($e \geq 0$), which must also satisfy the initial assumption that $e << 1$. Thus there is a steady state at the north pole only when *B* and G have different signs. This corresponds to the positive root in equation 4 when $B>0$ and the negative root when $B<0$. At the south pole,

$$-De^2 - Be + G = 0 \qquad (5)$$

$$e = \frac{+B \pm \sqrt{B^2 + 4DG}}{-2D} \qquad (6)$$

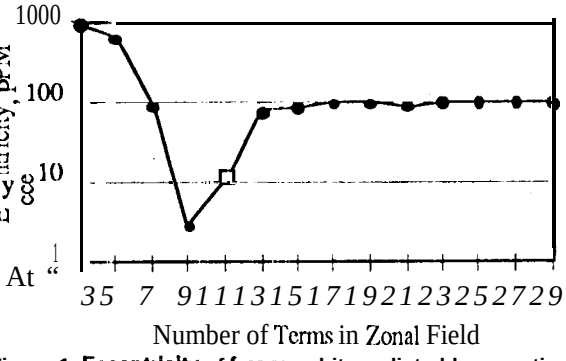

Figure 1. Eccentricity of frozen orbit predicted by equation 7 for TOPEX/Poseidon as a function of the number of terms in the zonal potential. Dots: north pole; Square: south pole solution.

The south pole solutions exist when both *B* and G have the same sign, corresponding to the positive root in equation 6 when they are both negative, and the negative root when they arc both positive. At this point equations 4 or 6 could themselves be studied for bifurcations in terms of the parameters *B, D,* and G; however, these arc already fixed fro the problem at hand (the TOPEX/Poseidon orbit," $B \approx -9.105 \times 10^{-3}$ sec^{-1}, $G \approx 9.094 \times 10^{-12}$ sec^{-1}, and $D \approx 4.874 \times 10^{-10}$ sec^{-1}) and this problem is left for further study. Since $DG << B^2$ at inclinations sufficiently far away from the critical inclination (where $B=0$) equations 4 or 6 can be expanded as a series in the small parameter DG/B^2 to give

$$e_{ss} \approx -\frac{G}{B} = \frac{-\sin i \sum_{odd\ \ell} J_\ell \left(\frac{R_e}{a}\right)^\ell P_{\ell-1}(0) P'_\ell(\cos i)}{\sum_{even\ \ell} J_\ell \left(\frac{R_e}{a}\right)^\ell P_\ell(0)\left[\frac{\ell(\ell+1)}{2} P_\ell(\cos i) + \cos i P'_\ell(\cos i)\right]} \qquad (7)$$

A similar result has been given by Rosborough and Ocampo.[12] Since equation 7 was derived by assuming the $e << 1$, it is not valid if it gives an eccentricity approaching 1 (or larger). It is of vital importance to

[m] All values quoted in this paper for TOPEX/Poseidon are based upon a truncation of the GEM-T3 gravity field at J29.

include a sufficient number of terms in the expansion; this is illustrated in figure 1 for the TOPEX/Poseidon orbit. If the calculation had stopped with J9, the predicted eccentricity would be nearly two orders of magnitude too small, while if it had stopped at J 11, the frozen orbit would have been predicted in the wrong hemisphere! It appears from figure 1 that a minimum of 13 terms arc required for this satellite.

Equation 7 has a singularity at the "critical inclination" which occurs when $\mathrm{Cos}^2 i \approx 1/5$, corresponding to an inclination of approximately $i_{critical} \approx 63.435°$. Near this inclination, the approximation that $DG << B^2$ is invalid, since $B \approx 0$. It is possible to get higher eccentricity frozen orbits near this inclination. At a slightly larger inclination, G also passes through zero. In the range of inclinations between the two zeroes, frozen orbit solutions exist at the south pole. The critical inclination has been studied extensively elsewhere.[23] For TOPEX/Poseidon $e_{ss} \approx 99.88$ PPM. Furthermore, there is a second singularity in the derivation when $D=O$, at an inclination of ≈32.4°, which also demands further analysis.

PHASE PORTRAIT OF THE FROZEN ORBIT

The system of differential equations 1 and 2 can be directly integrated to give trajectories in phase space. This is fortunate, since the system is non-hyperbolic (has purely imaginary eigenvalues) and the Hartman-Grobman theorem (the flows of the nonlinear system arc homomorphic to the linear system in some neighborhood of the steady state) does not apply. Unless onc can find a Lyapunov function, there is no easy analytic method to dctcrminc stability, hence the usual introduction of numerical integration, Later, when non-gravitational perturbations arc introduced, the resulting structural instability of the system will perturb the circular centers seen here into either spiral centers (stable or unstable) or saddle nodes.

Consider the pair (e,ω) as the polar coordinates of a vector whose Cartesian representation is

$$x = e\cos\omega \tag{8}$$

$$y = e\sin\omega \tag{9}$$

Then

$$\dot{x} = \dot{e}\cos\omega - e\dot{\omega}\sin\omega = \frac{\dot{e}}{e}x - \dot{\omega}y = \frac{x}{e}(-G\cos\omega) - y\left(B + \frac{G}{e}\sin\omega\right) = -G - By \tag{10}$$

$$\dot{y} = \dot{e}\sin\omega + e\dot{\omega}\cos\omega = \frac{y}{e}\dot{e} + x\dot{\omega} = \frac{y}{e}(-G\cos\omega) + x\left(B - \frac{G}{e}\sin\omega\right) = Bx \tag{11}$$

Taking the ratio of the last two equations gives

$$\frac{dy}{dx} = \frac{-Bx}{G + By} \tag{12}$$

integrating and completing the squares in y,

$$X^2 + (y - e_{ss})^2 = C^2 \tag{13}$$

where $e_{ss} = -G/B$ and C is a constant determined by the initial conditions. Equation 13 describes a family of circles centered at (O, e_{ss}). Figure 2 illustrates one typical such family, based on the J3 truncations of B and G for TOPEX/Poseidon. The only difference between the family shown in figure 2 and the complete family is the location of the center. North pole frozen orbits will have centers in the top half plane, while south pole frozen orbits will have centers in the bottom half plane. Transforming back to orbital coordinates,

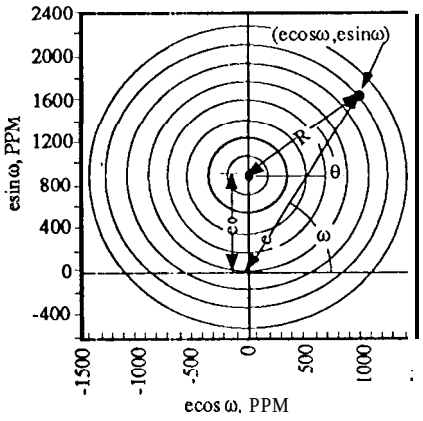

Figure 2. Frozen orbit trajectories described by equation 5 for TOPEX/Poseidon to J3.

$$e^2\cos^2\omega + \left(e\sin\omega + \frac{G(a,i)}{B(a,i)}\right)^2 = C^2 \tag{14}$$

The phase portrait predicted by equation 14, following the first TOPEX/Poseidon orbit maintenance maneuver, is illustrated in figure 2. The contours described by both equations 13 and 14 arc closed. The steady state is thus a "center point" of trajectories with periodic variations in eccentricity and argument of perigee. This periodicity arises from a Hopf bifurcation which occurs when the magnitude of non-gravitational disturbing forces (e.g. drag) goes to zero.

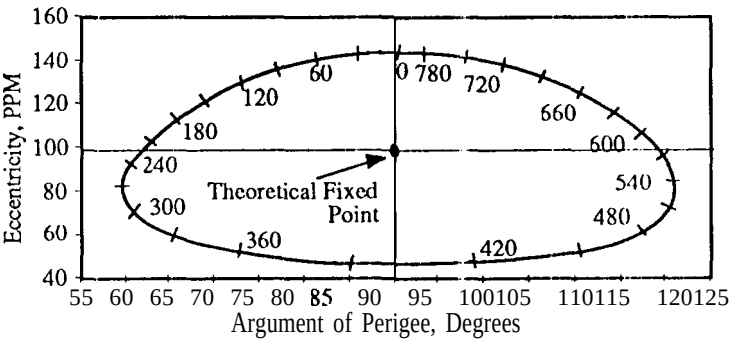

Figure 3. Frozen orbit predicted for TOPEX/Poseidon after the first orbit maintenance maneuver. The tick marks sre in days. Non-gravitational forces and subsequent maneuvers are not Included.

Calculation of the eigenvalues provides explicit formulas for the period of oscillation of the linearized system. The Jacobian matrix of equations 1 and 2, evaluated at the north polar steady state is

$$J(e_{ss},90^\circ)=\left[\begin{matrix}\left[\frac{G}{e}+eD\right]\cos\omega & \left[D-\frac{G}{e^2}\right]\sin\omega \\ A\sin\omega & 0\end{matrix}\right]_{\substack{e=-G/B\\ \omega=90^\circ}}=\begin{bmatrix}0 & -\frac{B^2}{G}\\ G & 0\end{bmatrix} \tag{14}$$

where the approximation $B^2/G>>D$ (only vafid outside of a neighborhood of the critical inclination, see equation A36 in the appendix) and the result $G=A$ *(see the* discussion following equation A31) have been used. The eigenvalues arc the roots of the characteristic equation

$$0=\det(J-\lambda I)=\lambda^2+B^2 \tag{15}$$

hence

$$\lambda=\pm i|B| \tag{16}$$

Thus the period of oscillation is

$$\tau=\frac{2\pi}{|B|}=2\pi\left|\sum_{even\ \ell} nJ_\ell\left(\frac{R_e}{a}\right)^\ell P_\ell(0)\left[\frac{\ell(\ell+1)}{2}P_\ell(\cos i)+\cos iP'_\ell(\cos i)\right]\right|^{-1} \tag{17}$$

giving a period of approximately 26 months for TOPEX/Poseidon.

NON-GRAVITATIONAL FORCES

Atmospheric Drag

Incorporating the effects of a drag perturbation into equations 1 and 2 gives to lowest order in the eccentricity (see equations A50 and A55 in the appendix)

$$\frac{d\omega}{dt}=B+\frac{G}{e}\sin\omega-\frac{K\rho_5}{e} \tag{18}$$

$$\frac{de}{dt}=-A\cos\omega-\rho_1K-p2Ke \tag{19}$$

The perturbed steady states are

$$\cos\omega = -\frac{K}{B}(\rho_1 + e\dot{\rho}_2) \tag{20}$$

$$e = e_{ss}\sin\omega - e_{ss}\frac{\mathrm{Kp5}}{G} \tag{21}$$

Defining $\Delta\omega=\omega-\pi/2+\Delta$ and $\delta e=e-e_{ss}$ and assuming that the perturbations are small,

$$\sin\omega = \sin(\pi/2 + \Delta\omega) = \cos\Delta\omega \approx 1 - (\Delta\omega)^2/2 + \ldots \tag{22}$$

$$\cos\omega = \cos(\pi/2 + \Delta\omega) = -\sin\Delta\omega \approx -\Delta\omega + \cdots \tag{23}$$

then

$$\& \approx -e_{ss}K\rho_5/B \tag{24}$$

$$\Delta\omega \approx \frac{K}{G}(\rho_1 + p2e) \tag{25}$$

Since $\delta e/e_{ss} \approx -K\rho_5/B << 1$ *the* approximation e $\approx e_{ss}$ can be used in the right hand side of equation 25. For TOPEX/Poseidon, $B\approx$-9.105×10^{-8} see-l, $G\approx$9.094×10^{-12} See-l, $K \approx$ 9.86x 10^{-8} km^3 /kg – scc, *and* $p \approx 4$ x 10^{-7} kg/km^3 (orbital avtx-age, low flux, Jacchia-Roberts at mospheric model[24]). Hence $|K\rho_5|$ <4 x 10^{-14} sec'*. The Jacobian of the perturbed system is then

$$J = \begin{bmatrix} \frac{G}{e}\cos\omega & -\frac{G}{e^2}\sin\omega + \frac{K\rho_5}{e^2} \\ G\sin\omega & -K\rho_2 \end{bmatrix} \approx \begin{bmatrix} -\frac{G\Delta\omega}{e_{ss}} & -\frac{G}{e_{ss}^2} \\ G & -K\rho_2 \end{bmatrix} \tag{26}$$

and the characteristic equation of the linearized system is

$$\lambda^2 + (G\Delta\omega/e_{ss} + \rho_2 K)\lambda + (G/e_{ss})(\rho_2 K\Delta\omega + G/e_{ss}) = O \tag{27}$$

The eigenvalues arc

$$\lambda = \frac{1}{2}\left\{-(K\rho_2 + G\Delta\omega/e_{ss}) \pm \sqrt{(K\rho_2 + G\Delta\omega/e_{ss})^2 - 4(G/e_{ss})(\rho_2 K\Delta\omega + G/e_{ss})}\right\} \tag{28}$$

Since the function defined by equation 28 is continuous and

$$\lim_{\rho\to 0}\lambda = \pm\sqrt{G^2/e_{ss}^2} = \pm iB \tag{29}$$

the conditions for a Hopf bifurcation are met. Hence one expects oscillatory behavior to occur in the (e,ω) plane. The condition for stability is that the real part of the eigenvalue be negative, i.e.,

$$Kp2 + G\Delta\omega/e_{ss} > 0 \tag{30}$$

Substituting equation 25 gives

$$\rho_2(1 + e/e_{ss}) > -\rho_1 \tag{31}$$

These oscillations will produce stable spirals when this condition is met. For the typical satellite orbits we arc considering the density[24] peaks at $\approx 14^h00^m$ local time, and can be pheonmenologically represented by

$$p(E) = \bar{\rho} + \delta\rho\cos(E - E_{\max}) \tag{32}$$

where $\bar{\rho}$ and $\delta\rho$ *are* positive constants and $E_{\max}$ is the eccentric anomaly at maximum density. Then since $\rho_1 \approx (\delta\rho/2)\cos E_{\max}$ and $p_2 \approx \bar{\rho}$,

$$\rho_2(1 + e/e_{ss}) + \rho_1 > \rho_2 + \rho_1 = \bar{\rho} + (\delta\rho/2)\cos E_{\max} > \bar{\rho} - (\delta\rho/2) > 0 \quad \Leftrightarrow \quad \delta\rho < 2\bar{\rho} \qquad (33)$$

Since $1 + e/e_{ss} \approx 2$, values of $\delta\rho$ as large as $\approx 4\bar{\rho}$ will usually be sufficient to guarantee that equation 30 is satisfied and the perturbed phase plane trajectories are stable. For TOPEX/Poseidon at low flux values, $\bar{\rho} \approx 4 \times 10^{-7} kg/km^3$, $\delta\rho \approx 2 \times 10^{-7} kg/km^3$ (using a Jacchia-Robert.$~ model) and hence the stronger condition is easily met. Thus drag should have a stabilizing influence.

Constant Density Atmosphere

When the density ρ is fixed over the entire orbit, equations 18 and 19 bccomc

$$\frac{d\omega}{dt} = B + \frac{G}{e}\sin\omega \qquad (34)$$

$$\frac{de}{dt} = -G\cos\omega - \frac{1}{2}\rho K e \qquad (35)$$

and the ncw steady state is

$$\hat{\omega} = \text{tan-l}\left(2G/K\rho e_{ss}\right) \qquad (36)$$

$$\hat{e} = e_{ss}\Big/\sqrt{1 + \left(\rho K e_{ss}/2B\right)^2} \qquad (37)$$

For TOPEX/Poseidon, G ≈ 9.094 x 10^{-12} see-l, $A \approx 15m^2$, and $K \approx 9.86\text{x } 10^{-8} km^3$ /kg – sec, hence $\Delta\omega = 90° - \hat{\omega} \approx 1\ 25\text{"x}10^{-5}$. A shift in perigee by as much as one degree would require a density of 33 gm/km^3, corresponding to the maximum Harris-Priester density[25] at 300 km. Thus drag does not significant y affect the frozen orbit for TOPEX/Poseidon. The Jacobian at the new steady state $(\hat{e}, \hat{\omega})$ is

$$J(\hat{e},\hat{\omega}) = \left[\begin{matrix} \frac{G}{e}\cos\omega & -\frac{G}{e^2}\sin\omega \\ G\sin\omega & -\frac{1}{2}\rho K \end{matrix}\right]_{\substack{e=\hat{e} \\ \omega=\hat{\omega}}} = \left[\begin{matrix} -\frac{\rho K}{2} & \frac{G}{\hat{e}e_{ss}} \\ -\frac{G\hat{e}}{e_{ss}} & -\frac{\rho K}{2} \end{matrix}\right] \qquad (38)$$

and hence the eigenvalues form a complex conjugate pair

$$\lambda = -\frac{\rho K}{2} \pm i|B| \qquad (39)$$

Since the real parts of the eigenvalues arc negative, the trajectories form stable spirals. Hence the effect of drag in a constant density atmosphere on the frozen orbit is stabilizing.

Continuous Along-Track Thrust

Shortly after the TOPEX/Poseidon launch, analysis of orbital data revealed the presence of hitherto unexpected accelerations causing a decay in the semi-major axis as much, as 60 times larger than could be explained by atmospheric drag, These accelerations steadily declined over the next six weeks to a residual level which was approximately seven to ten times larger than drag in magnitude, varied with yaw mode, and alternated between orbital decay and boost.[26] The original accelerations have since been attributed to outgassing, while the residual accelerations have been attributed to non-symmetrical radiation exposure of the solar array over a single orbit and thermal radiation being emitted by the satellite.[270M] These accelerations display characteristics of continuous low-level along-track thrust forces on the order of several rnicro-newtons.

Applying a continuous along-track thrust to equations 1 and 2 gives (see equations A57 and A58)

$$\frac{d\omega}{dt} = B + \frac{G}{e}\sin\omega \qquad (40)$$

$$\frac{de}{dt} = -G\cos\omega - \frac{2T}{mv}e \qquad (41)$$

These arc completely analogous to equations 34 and 35 for a constant-density drag, with $\rho K / 2$ replaced by $2T / mv$. This is not too surprising{; since drag acts along the direction of motion. Consequently,

$$\hat{\omega} = \tan\text{-}1\left(mvG/2Te_{ss}\right) \tag{42}$$

$$\hat{e} = e_{ss}\Big/\sqrt{1+\left(2Te_{ss}/mvB\right)^2} \tag{43}$$

For typical TOPEX/Poseidon parameters and a force of 2. $\mu N, \Delta\omega \approx 0.14$". A change of perigee by onc degree would require a thrust of 14 μN. Onc significant difference between a continuous thrust and a constant drag is that the thrust can be applied in either direction, while the density is non-negative. Thus a continuous thrust can be either stabilizing or destabilizing. Furthermore, while the concept of a Hopf bifurcation was just a useful mathematical fiction realizable only in the limit of zero drag, thrust provides a physically realizable Hopf bifurcation.

Solar Radiation Pressure

Solar radiation pressure (SRP) changes equations 1 and 2 to (see equations A63 and A70)

$$\frac{d\omega}{dt} = B + \frac{G}{e}\sin\omega + \frac{W}{e} \tag{44}$$

$$\frac{de}{dt} = -G\cos\omega + H \tag{45}$$

where H and W arc functions of the solar direction vector with respect to the orbit plane. The steady state at each pole bifurcates into a pair of states $\left(\tilde{e}_{\pm}, \tilde{\omega}\right)$ such that

$$\tilde{\omega} = \cos^{-1}(H/G) \tag{46}$$

$$\tilde{e}_{\pm} = -\frac{W}{B} \pm \frac{1}{B}\sqrt{G^2 - H^2} \tag{47}$$

These steady states may not be physically realizable, however. For the eccentricity to be real-valued immediately gives

$$|H/G| \le 1 \tag{48}$$

If this condition is not met then no steady state solutions exist. Furthermore, the eccentricity must be positive. For $\tilde{e}_+$ to exist, this is equivalent to

$$W < \sqrt{G^2 - H^2}, \quad B > 0 \tag{49}$$

$$W > \sqrt{G^2 - H^2}, \quad B < 0 \tag{50}$$

For $\tilde{e}_-$ to exist, the equivalent conditions to equations 49 and 50 are

$$W < -\sqrt{G^2 - H^2}, \quad B > 0 \tag{51}$$

$$W > -\sqrt{G^2 - H^2}, \quad B < 0 \tag{52}$$

The Jacobian at the steady states is

$$J = \begin{bmatrix} \left(G/\tilde{e}_{\pm}\right)\cos\tilde{\omega} & -\left(G/\tilde{e}_{\pm}^2\right)\sin\tilde{\omega} - W/\tilde{e}_{\pm}^2 \\ G\sin\tilde{\omega} & 0 \end{bmatrix} = \begin{bmatrix} H/\tilde{e}_{\pm} & B/\tilde{e}_{\pm} \\ -\left(\tilde{e}_{\pm}B + W\right) & 0 \end{bmatrix} \tag{53}$$

which has eigenvalues at

$$\lambda = \frac{H}{2\tilde{e}_{\pm}} \pm \frac{1}{2}\sqrt{\left(H/\tilde{e}_{\pm}\right)^2 - 4\left(B^2 + BW/\tilde{e}_{\pm}\right)} \tag{54}$$

There is a Hopf bifurcation when H and W pass through zero simultaneously, or when H passes through zero while $B^2 + BW/\tilde{e}_{\pm} > 0$. If

$$B^2 + BW/\tilde{e}_{\pm} < 0 \tag{55}$$

the critical points will be saddle nodes, If the argument of the square root is negative and $H<0$, the steady state will be a stable spiral center; if H >0, and unstable spiral center. As the argument of the square root in equation 54 passes through zero with $H\neq0$, a saddle-node bifurcation occurs. The condition for centers is

$$W < \frac{G^2 - 1.2511^2}{\sqrt{G^2 - H^2}} \qquad e = \tilde{e}_+ \tag{56}$$

$$W > \frac{1.25F^2 - 11^2}{\sqrt{G^2 - H^2}} \tag{57}$$

These results are summarized in figure 4. While the value of *B is* essentially fixed for any satellite (assuming semi-major axis and inclination do not change), *W* and H are dynamic functions of the solar geometry. As the geometry changes, the value of (H, *W*) moves through the *H/W* plane. Whenever the point (*H*,*W*) crosses regional boundaries, the nature of the steady state changes. So long as (*H*, *W*) remains in the shaded areas, the critical point (the steady state of eqns. 44 and 45 in (e,ω) space) be a spiral center; if (*H*,*W*) crosses into the lined area, the steady state becomes a saddle node. The spiral center is stable when (*H*,*W*) is on the left half plane, and unstable when (*H*,*W*) is on the right half plane. If (*H*,*W*) passes into the unshaded area, the steady state disappears entirely. There is potentially a very complicated dynamic, with the stead y state alternatel y stable, unstable, bifurcating, or disappearing entirel y.

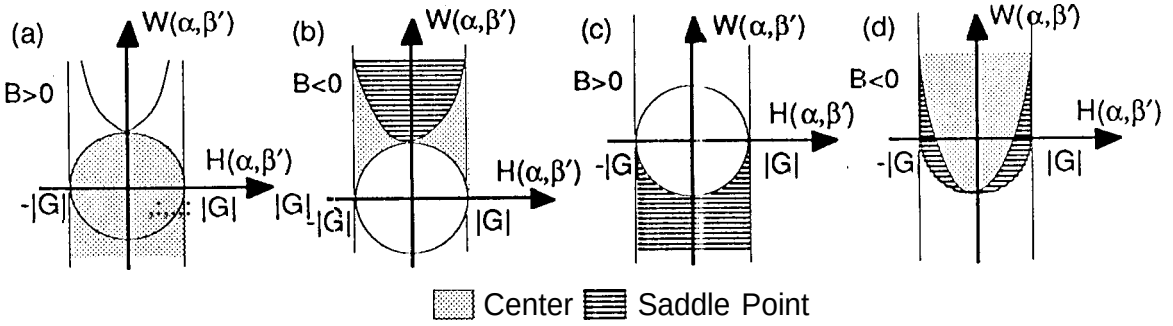

Figure 4. Bifurcation parameter space for SRP, with *W* and *H*, defined by equations A63 and A70, treated as parameters. (a) and (b): parameter space for e_+; (c) and (d): parameter space for e..

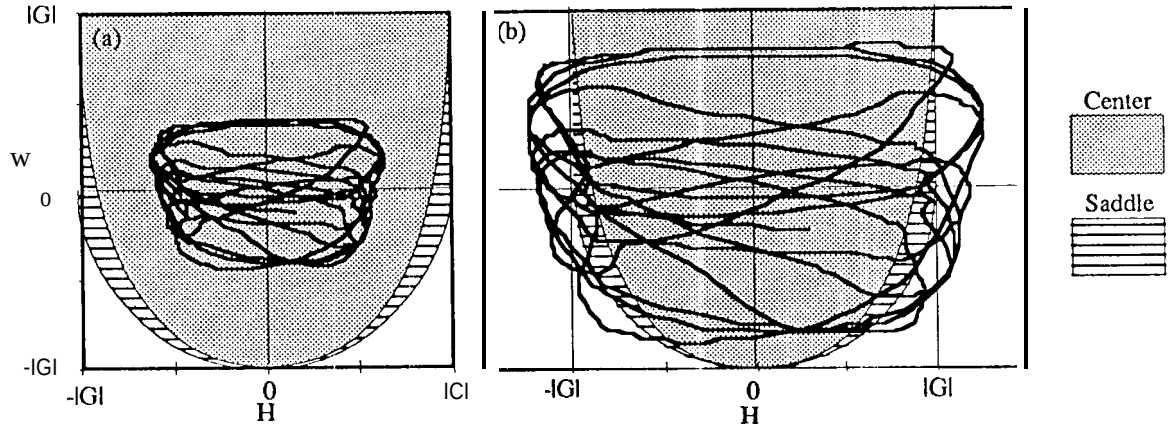

Figure 5. Parameter apace evolution corresponding to figure 4d for the TOPEX/Poseidon primary mission. (a) Actual orbit. (b) Hypothetical satellite with one half the mass of TOPEX/Poseidon.

For TOPEX/Poseidon, $B \approx -9.105\times10^{-8}\ \mathrm{sec}^{-1}$ and $G \approx 9.094\times10^{1}$, hence the possible situations are those illustrated in figure 6b for $\tilde{e}_+$ and figure 6d for Z_. The effect of solar radiation pressure on the steady state is illustrated by figures 5 and 6. Figure 5a shows the variation in the *H/W* plane. Since the location of (*H*, *W*) is always within the circle of radius ICI, the steady state at $\tilde{e}_+$ does not exist. Figure 6a shows the variation of the steady state at $\tilde{e}_-$ resulting from this motion in the *H/W* plane; it

alternates between stable and unstable spirals 'with a period of approximately 56 days. The predicted variation of the actual orbital parameters for the three year primary mission, ignoring maneuvers, is shown in figure 6b. The mean clement propagations illustrated in figures 6 and 7 were performed using GTARG* which has been described elsewhere.[28] GTARG has been updated to account for the perturbations on the frozen orbit described in the appendix. From equations A63 and *A-JO* in the appendix, the variation in the H/W plane is inversely proportional to the satellite mass. Halving the mass would double the rate of variation; the evolution of such a hypothetical system in the *n/W* parameter plane is shown in figure 5b, and in the (e,ω) phase plane in figure 7. In this case the system passes through all three regions of the parameter plane, stable/unstable spiral, saddle, and total non-existence of a stationary point.

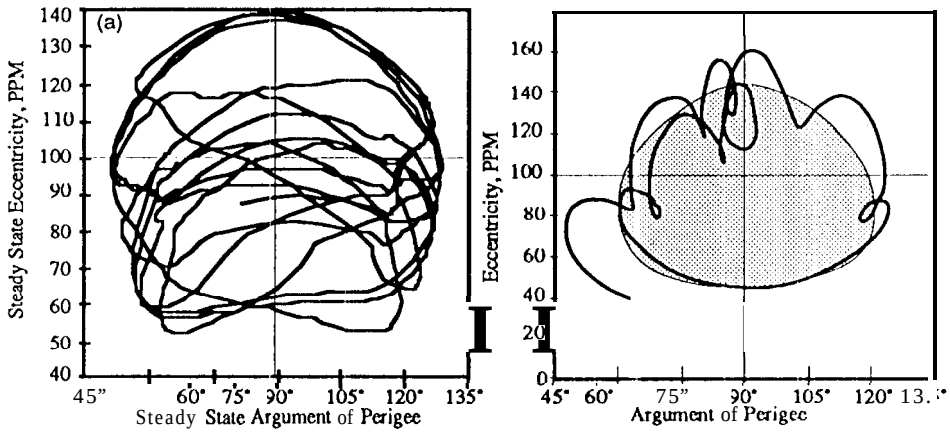

Figure 6. Effect of solar radiation pressure on TOPEX/Poseidon frozen orbit over three year primary mission. (a) Variation of steady state. (b) Predicted evolution of frozen orbit Ignoring maneuvers. The unperturbed curve encloses the shaded area.

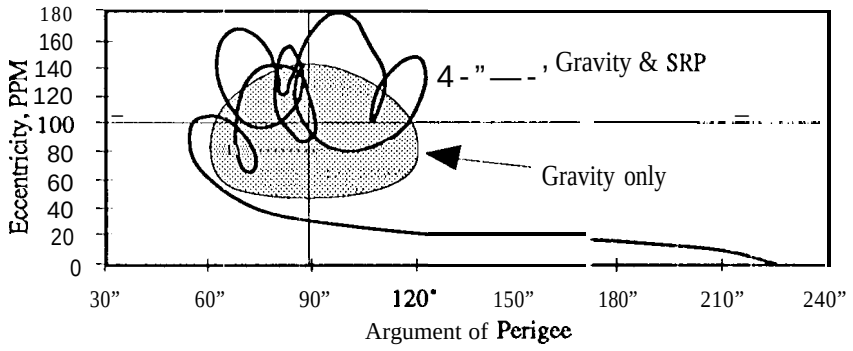

Figure 7. Predicted evolution In (e, ω) phase plane for the hypothetical satellite of figure 5b.

OBSERVATIONS

Operational orbit determination for TOPEX/Poseidon is provided by the Goddard Space Flight Center Flight Dynamics Division (GSFC/FDD) using GTDS[25] to process observations obtained via the TDRSS.[29] Mean elements arc calculated by removing all central body zonal, sectorial, and tesseral harmonics, second-order J2, and third-body (luni-solar) perturbations acting over a specified time interval, as described by Guinn.[30] An analysis of variations in the observed orbit, particularly a and i, has been prcscntcd previously.[31] In summary, the frozen orbit was maintained throughout the TOPEX/Poseidon

" GTARG is available from COSMIC.* A description is available on the World Wide Web at URL http://www.cosmic.uga.edu.

prime mission without requiring any dedicated maneuvers. Although eight orbit maintenance maneuvers (OMM) were performed during this period to recover semi-major axis decay due to drag and maintain the exact repeat ground track, every effort was made to not increase e when performing an OMM. The predicted evolution of the frozen orbit after each maneuver is illustrated in figure 8. The corresponding ob.served mean elements derived from the GSFC/FDD TDRSS observations are summarized in figures 9 through 11. Figure 9 shows the observations in the x/y phase plane described earlier, with post-maneuver predictions, including all of the perturbations described in the appendix as predicted by GTARG. The unperturbed (gravity-only) solution is also shown. While it is not possible to see trends from figure 9 due to the density of data points, it dots clearly demonstrate that the frozen orbit has remained relatively close to the gravity-only solution (the circle in figure 9). The actual

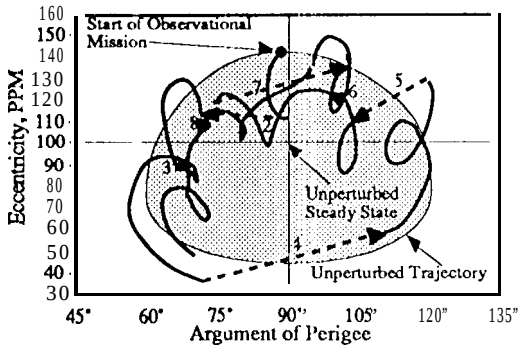

Figure 8. Frozen orbit following each maneuver as predicted by GTARG. Orbit maintenance maneuvers (OMM) are annotated sequentially.

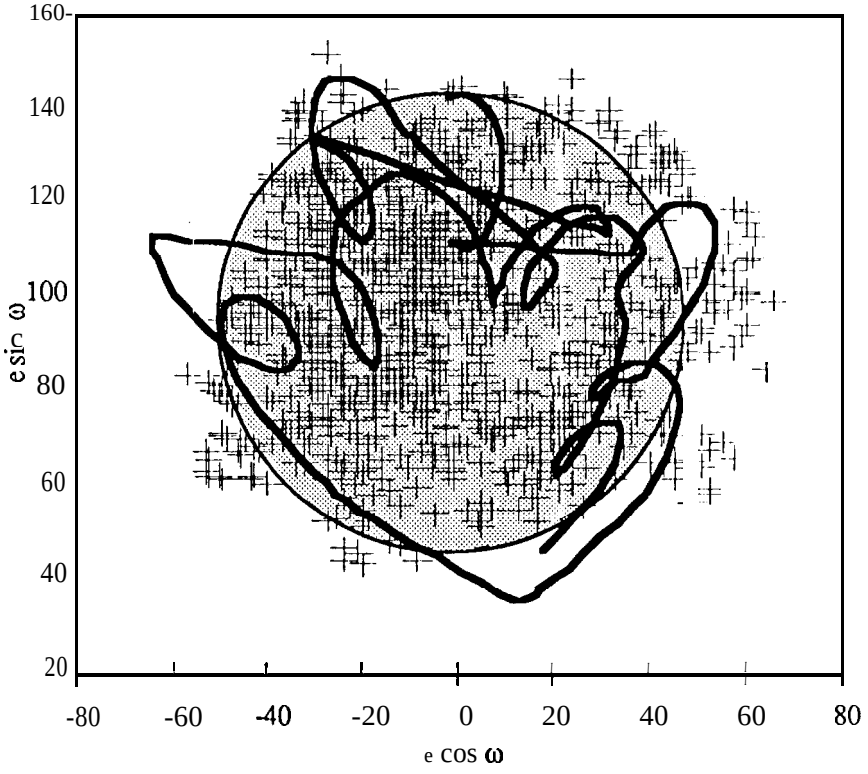

Figure 9. Observed and predicted frozen orbit for TOPEX/Posefdon. The boid curve is identical to the boid curve of figure 8, but Is plotted in the (ecosω, esinω) coordinate plane rather than the (e,ω) plane. The symbols show observed values of the orbital elements. The shaded areas of figure 8 and figure 9 correspond to the came area of phase space and are bordered by the gravity-only solution given by equations 13 and 14. The shading is not significant, but Is added for clarity.

evolution of the frozen orbit as a function of time is illustrated in figure 10. Figure 10a shows the observed and predicted eccentricity as a function of time. The mean eccentricity derived from FDD observations is shown by the light-weight curve, the gravity-only prediction at the start of the prime mission is indicated by the medium-weight curve, and the post-maneuver predictions including all

perturbations modeled in the appendix by the heavy-weight curve. The effect of solar radiation pressure is clear from the figure.

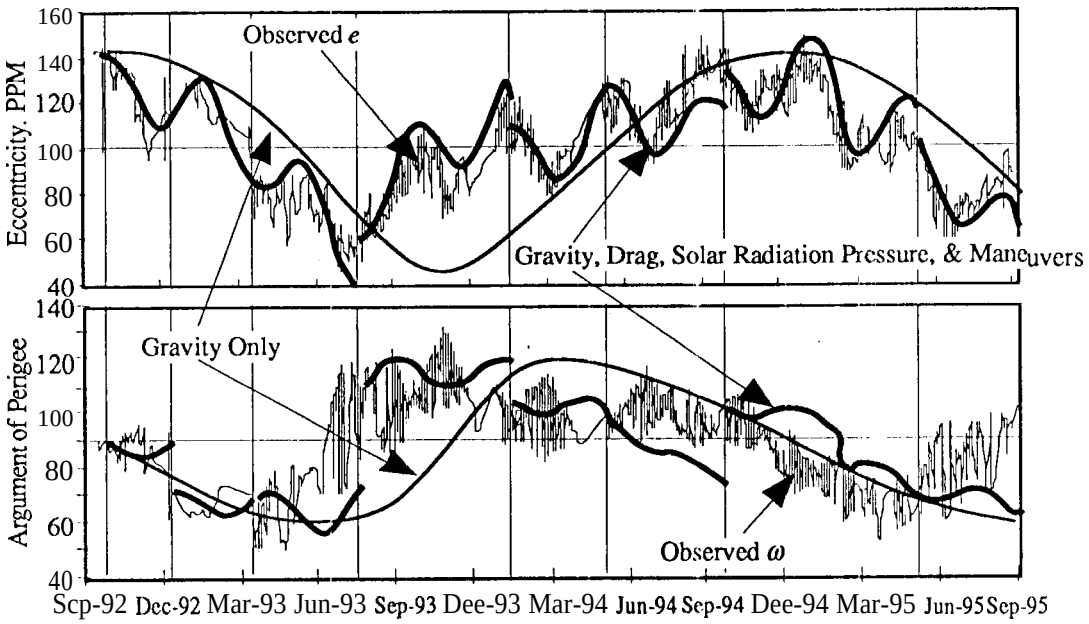

Figure 10. Observed and modeled TOPEX/Poseidon frozen orbit. Tick marks correspond to the 15th of the month. Maneuvers are Indicated by vertical grid lines.

SUMMARY

The low eccentricit y frozen orbit arises from a Hopf bifurcation when perturbing forces, such as atmospheric drag, solar radiation pressure, or along-track thrust, pass through zero. Drag has a stabilizing effect, while thrust can be either stabilizing or nonstabilizing. Solar radiation pressure is the most significant non-gravitational perturbation for TOPEX/Poseidon. It can cause the frozen orbit to repeatedly pass through both the Hopf bifurcation and a second saddle/node bifurcation, causing the steady state to alternatly be a stable spiral center, an unstable spiral center, and a saddle point. The result is a complicated phase trajectory which repeatedly loops back upon itself. For TOPEX/Poseidon the saddle/node bifurcation is never crossed and consequently the observed trajectory is never very far from the perturbation-free frozen orbit (drag and solar radiation pressure equal to zero), even when the effect of maneuvers for semi-major axis maintenance arc taken into account. The effects of luni-solar gravity, non-spherical solar reflection, and differential black-body radiation have not been considered and may account for some of the difference between the predicted and observed phase portraits. Nevertheless, the TOPEX/Poseidon satellite continues in a frozen orbit at the end of its primary three-year mission, although not a single eccentricity-maintenance maneuver was required. During this same period a total of eight drag make-up maneuvers were performed.

ACKNOWLEDGEMENTS

Useful criticisms of this manuscript were given by Carl Christensen and Ray Frauenholz of the Jet Propulsion Laboratory. Many thanks are due to Shannon Coffey of NRL for promptly responding to my queries, and to James Sncyd of the University of Canterbury, New Zealand for bringing the beauty of bifurcation theory to my attention, albeit in a very different context.

APPENDIX - PERTURBING FORCES

Zonal Gravity Field

The general zonal perturbations on the mean eccentricity y and argument of perigee arc given[21,22] in terms of the Legendre Polynomials*,[32] as

$$\frac{d\omega}{dt} = -\sum_{\ell=2}^{\infty} nJ_\ell \left(\frac{R_e \xi}{a}\right)^\ell \sum_{k=0}^{\ell} \frac{(\ell-1)!}{(\ell+k-1)!} \cos\left[k\left(\omega-\frac{\pi}{2}\right)\right] \times \left\{\left[\left(\ell+\frac{k}{e^2}\right)P_{\ell-1}^k(\xi)+\frac{1}{e}P_{\ell-1}^{k+1}(\xi)\right]V_{\ell k}^0(i)-2\cot i\, P_{\ell-1}^k(\xi)E_{\ell k0}^0(i)\right\} \tag{A1}$$

$$\frac{de}{dt} = -\sum_{\ell=2}^{\infty} \frac{nJ_\ell}{e}\left(\frac{R_e \xi}{a}\right)^\ell \sum_{k=1}^{\ell} ku_k \sin\left[k\left(\omega-\frac{\pi}{2}\right)\right] \frac{(\ell-k)!(\ell-1)!}{(\ell+k)!(\ell+k-1)!} T_\ell^k(0) T_\ell^k(\cos i) P_{\ell-1}^k(\xi) \tag{A2}$$

Where

$$\xi = \left(1-e^2\right)^{-1/2} \tag{A3}$$

$$u_k = 2-\delta_{k0} \tag{A4}$$

$$V_{\ell k}^0(i) = u_k \frac{(\ell-k)!}{(\ell+k)!} T_\ell^k(\cos i) T_\ell^k(0) \tag{AS}$$

$$E_{\ell k0}^0(i) = \frac{1}{2} u_k \frac{(\ell-k)!}{(\ell+k)!} T_\ell^k(0)\left[k\cot i\, T_\ell^k(\cos i) - T_\ell^{k+1}(\cos i)\right] \tag{A6}$$

Equations A 1 and A2 are considerably simplified in the low e approximation. From A3, when e<< 1

$$\left(1-\xi^2\right)^{k/2} \approx (-1)^{k/2} e^k \tag{A7}$$

Hence

$$P_{\ell-1}^k(\xi) = (-1)^{k/2}\left(1-\xi^2\right)^{k/2} P_{\ell-1}^{(k)}(\xi) \approx e^k P_{\ell-1}^{(k)}(1) = \delta_{k0} + \frac{1}{2} e\ell(\ell-1)\delta_{k1} + O(e^2) \tag{A8}$$

where the fact that $P_\ell(1) = 1$ and $Q'(1) = \ell(\ell+1)/2$ have been used.[32] Combining the last two results

$$P_{\ell-1}^{k+1}(\xi) = (-1)^{(k+1)/2}\left(1-\xi^2\right)^{(k+1)/2} P_{\ell-1}^{(k+1)}(\xi) \approx e^{k+1} P_{\ell-1}^{(k+1)}(1) = \frac{1}{2} e\delta_{k0}\ell(\ell-1) \tag{A9}$$

Substituting equations AS and A9 into equation Al gives, to lowest order in e,

$$\frac{d\omega}{dt} = -\sum_{\ell=2}^{\infty} nJ_\ell \left(\frac{R_e}{a}\right)^\ell \sum_{k=0}^{\ell} \cos\left[k\left(\omega-\frac{\pi}{2}\right)\right] \frac{(\ell-1)!}{(\ell+k-1)!} \times \left\{\left[\ell+\frac{k}{e^2}\right]\left(\delta_{k0}+\delta_{k1}\frac{e\ell(\ell-1)}{2}\right)+\delta_{k0}\frac{\ell(\ell-1)}{2}\right]V_{\ell k}^0(i)-2\cot i\, E_{\ell k0}^0(i)\Big\}\delta_{k0}+\delta_{k1}\frac{e\ell(\ell-1)}{2} \tag{A10}$$

The Kroeneker delta collapses the summation over k to only two terms:

$$\frac{d\omega}{dt} = -\sum_{\ell=2}^{\infty} nJ_\ell \left(\frac{R_e}{a}\right)^\ell \underbrace{\left\{\frac{(\ell-1)!}{(\ell-1)!}\left[\left[\ell+\frac{\ell(\ell-1)}{2}\right]V_{\ell 0}^0(i)-2\cot i E_{\ell 00}\right]\right\}}_{k=0} + \underbrace{\frac{(\ell-1)!}{a}\cos(\omega-\pi/2)\left\{\left(\ell+\frac{1}{e^2}\right)\ell(\ell-1)V_{\ell 1}^0(i)-2\cot i\, E_{\ell 10}\frac{e}{2}\ell(\ell-1)\right\}}_{k=1} \tag{A11}$$

---

* The associated Legendre Polynomials are defined as $P\}(x) = (-1)^{k/2} T_\ell^k(x)$ and $1\}(x) = 2\left(1-x\right)^{k/2}(\Phi)_\ell(x)$. The compact notation $P_\ell^{(k)}(\xi) = \left(d^k/dx^k\right)P_\ell(x)\Big|_{x=\xi}$ and $P_\ell'(\xi) = \left(dP_\ell(x)/dx\right)\Big|_{x=\xi}$ is used.

and hence

$$\frac{d\omega}{dt} = -\sum_{\ell=2}^{\infty} nJ_\ell \left(\frac{R_e}{a}\right)^{\ell} \left\{ \frac{\ell-1}{2} V^0_{\ell 0} - 2\cot i\, E^0_{\ell 00} + \left[\frac{\ell-1}{2e} V^0_{\ell 1} - e(\ell-1)\cot i\, E^0_{\ell 10} \right] F'S(6) \right\} \tag{A12}$$

The explicit dependence on inclination has been omitted from equation A12. To further and focus on the sensitivity to variations of e and ω, define the auxiliary functions

$$j_\ell(a) = nJ_\ell \left(\frac{R_e}{a}\right)^{\ell} \tag{A13}$$

$$\beta_\ell(i) = \frac{\ell(\ell+1)}{2} V^0_{\ell 0}(i) - E^0_{\ell 00}(i)\cot i \tag{A14}$$

$$\gamma_\ell(i) = \frac{\ell-1}{2} V^0_{\ell 1}(i) \tag{A15}$$

$$\delta_\ell(i) = (\ell-1) E^0_{\ell 10}(i)\cot i \tag{A16}$$

$$B(a,i) = -\sum j_\ell(a)\beta_\ell(i) \tag{A17}$$

$$G(a,i) = -\sum j_\ell(a)\gamma_\ell(i) \tag{A18}$$

$$D(a,i) = -\sum j_\ell(a)\delta_\ell(i) \tag{A19}$$

where all of the summations arc over the range $\ell=2$ to $\ell=\infty$. Equation A12 can bc written more compactly

$$\begin{aligned} \frac{d\omega}{dt} &= -\sum j_\ell(a) \left[\beta_\ell(i) + \frac{1}{e}\gamma_\ell(i) - e\delta_\ell(i)\left(\cos\omega - \frac{\pi}{2}\right) \right] \\ &= -\sum j_\ell(a)\beta_\ell(i) - \frac{1}{e}\cos\left(\omega - \frac{\pi}{2}\right)\sum j_\ell(a)\gamma_\ell(i) + e\cos\left(\omega - \frac{\pi}{2}\right)\sum j_\ell(a)\delta_\ell(i) \\ &= B(a,i) + \frac{G(a,i)}{e}\cos\left(\omega - \frac{\pi}{2}\right) - eD(a,i)\cos\left(\omega - \frac{\pi}{2}\right) \end{aligned} \tag{A20}$$

Similarly, substituting equation A 10 into equation A2 gives

$$\begin{aligned} \frac{de}{dt} &= -\sum_{\ell=2}^{\infty} \frac{nJ_\ell}{e} \left(\frac{R_e}{a}\right)^{\ell} \sin(\omega - \pi/2)\frac{(\ell-1)!(\ell-1)!}{(\ell+1)!\ell!} T^1_\ell(0) T^1_\ell(\cos i) e\ell(\ell-1) \\ &\quad - \sum_{\ell=2}^{\infty} nJ_\ell \left(\frac{R_e}{a}\right)^{\ell} \sin(\omega - \pi/2)\frac{\ell-1}{(\ell+1)} P_{\ell-1}(0) P'_\ell(\cos i)\sin i \end{aligned} \tag{A21}$$

Using equation 12 and defining the auxiliary functions (analogous to equations Al 3 through A14)

$$\alpha_\ell(i) = \frac{\ell-1}{\ell+1} P_{\ell-1}(0) P'_\ell(\cos i)\sin i \tag{A22}$$

$$A(a,i) = -\sum j_\ell(a)\alpha_\ell(i) \tag{A23}$$

equation A21 becomes

$$\frac{de}{dt} = -\sum j_\ell(a)\alpha_\ell(i)\sin\left(\omega - \frac{\pi}{2}\right) = A(a,i)\sin\left(\omega - \frac{\pi}{2}\right) \tag{A24}$$

To see that $DC << B^2$ away from the critical inclination, note that

$$P_{2n}(0) = (-1)^n \frac{1\cdot 3\cdot 5\cdots(2n-1)}{n!\,2^n} \tag{A25}$$

$$P_{2n+1}(0) = 0 \tag{A26}$$

Hence from equations A5 and A6,

$$V^0_{\ell 0}(i) = P_\ell(0)P_\ell(\cos i) \neq 0 \text{ only for } \ell \text{ even} \tag{A27}$$

$$E^0_{\ell 00}(i) = \frac{\sin i}{2} P'_\ell(\cos i) P_\ell(0) \neq 0 \text{ only for } \ell \text{ even} \tag{A28}$$

hence by equation A14, $\beta_\ell \neq 0$ only for/ even, and the sum in equation Al 7 is over/ even

$$B(a,i) = -\sum_{even\ \ell} nJ_\ell \left(\frac{R_e}{a}\right)^\ell P_\ell(0)\left[\frac{\ell(\ell+1)}{2}P_\ell(\cos i) + \cos i P'_\ell(\cos i)\right] \approx \frac{3nJ_2R_e^2\left(5\cos^2 i-1\right)}{2a^2} + \cdots \quad \text{(A29)}$$

Using the identity $(1-x^2)P'_n(X) = nP_{n-1}(x) - nxP_n(x)$, $P'_n(0) = nP_{n-1}(0)$, hence by equation A5

$$V^0_{\ell 1}(i) = \frac{2T^1_\ell(0)T^1_\ell(\cos i)}{\ell(\ell+1)} = \frac{2\sin i P'_\ell(0)P'_\ell(\cos i)}{\ell(\ell+1)} = \frac{2\sin i P_{\ell-1}(0)P'_\ell(\cos i)}{\ell+1} \neq 0 \text{ for } \ell \text{ odd} \quad \text{(A30)}$$

and hence

$$G(a,i) = -\sum_{odd\ \ell} nJ_\ell \left(\frac{R_e}{a}\right)^\ell \frac{\ell-1}{\ell+1} i P_{\ell-1}(0)P'_\ell(\cos i) \approx \frac{3nJ_3R_e^3 \sin i\left(5\cos^2 i-1\right)}{4a^3} + \cdots \quad \text{(A31)}$$

Comparing with equations A22 and A23 reveals that $A = G$ and hence

$$\frac{de}{dt} = -C(U,i)\cos\omega \quad \text{(A32)}$$

The ratio G/B, to order J3, is

$$-\frac{G}{B} = -\left[\frac{3nJ_3R_e^3 \sin i\left(5\cos^2 i-1\right)}{4a^3}\right] \Bigg/ \left[\frac{3nJ_2R_e^2\left(5\cos^2 i-1\right)}{2a^2}\right] = -\frac{J_3R_e \sin i}{2aJ_2} = e_3 \quad \text{(A33)}$$

where e_3 is the J3 stead y state eccentricity. To get an expression for D, evaluate equation A6 at $k = 1$,

$$\begin{aligned} E_{\ell 10} &= \frac{1}{\ell(\ell+1)} T^1_\ell(0)\left[\cot i T^1_\ell(\cos i) - T^2_\ell(\cos i)\right] \\ &= \frac{1}{(\ell+1)} P_{\ell-1}(0)\left\{\cos i P_{\ell-1}(\cos i) - (\ell-1)\sin^2 i P_{\ell-2}(\cos i)\right\} \end{aligned} \quad \text{(A34)}$$

Since $T_\ell(0) = P'_\ell(0)$, then by A6, $E^0_{\ell 10}(i) \propto P'_\ell(0) \propto P_{\ell-1}(0) \neq 0$ only when ℓ is odd. Hence from A19,

$$\begin{aligned} D(a,i) = -\sum_{\ell\ odd} nJ_\ell \left(\frac{R_e}{a}\right)^\ell \frac{\ell(\ell-1)}{\ell+1} P_{\ell-1}(0)\cot i\left\{\cos i P_{\ell-1}(\cos i) - (\ell-1)\sin^2 i P_{\ell-2}(\cos i)\right\} \\ \cdot \frac{3nJ_3R_e^3 \cos^2 i}{8a^3 \sin i}\left(7\cos^2 i - 5\right) + \cdots \end{aligned} \quad \text{(A35)}$$

and thus

$$|B/D| \approx |J_2/J_3| >> 1 >> e_3 = |G/B| \quad \text{(A36)}$$

demonstrating that DG/B^2 is small,* except near the critical inclination.

Non-Gravitationai Forces

Lagrange's planetary equations[33] give the effect of a velocity perturbation,

$$Ae = (1/na)\sqrt{1-e^2}\left[\Delta v_r \sin\theta + \Delta v_\theta (a/er)\left(1 - e^2 - r^2/a^2\right)\right] \quad \text{(A36)}$$

$$\Delta\omega = -(1/nae)\sqrt{1-e^2}\left[\Delta v_r \cos\theta + \Delta v_\theta (a/er)\left(1 + \frac{r}{a(1-e^2)}\right)\sin\theta + \Delta v_L \frac{r}{a}\cot i \sin(\omega+\theta)\right] \quad \text{(A37)}$$

Expanding to first order in eccentricity,

$$Ae \approx (1/na)\left[\Delta v_r \sin\theta + (2 - e\cos\theta)\Delta v_\theta \cos\theta\right] \quad \text{(A38)}$$

$$\Delta\omega \approx (-1/nae)\left[\Delta v_r \cos\theta + \Delta v_\theta \sin\theta(2 - e\cos\theta) + \Delta v_L e \cot i \sin(\omega+\theta)\right] \quad \text{(A39)}$$

---

* The ratio has a singularity when $\cos^2 i = 5/7$ (i= 32.37°) or for perfectly polar orbits, and hence the assertion may be false there as well as at the critical inclination. TOPEX/Poseidon has an ordination of 66.04° so this difficulty does not arise.

Then introduce a change of variables

$$\Delta v = \frac{F}{m}\frac{\Delta t}{\Delta M}\frac{\Delta M}{\Delta E}\Delta E \approx \frac{F}{}(1 - e\cos E)\Delta E \tag{A40}$$

The second half of equation A40 is obtained by differentiating Euler's equation

$$M = n(t - T) = E - e\cos E \tag{A41}$$

giving,

$$n = dM/dt = (1 - \mathrm{e}\cos E)\,dE/dt \tag{A42}$$

Finally, the transformations

$$\cos \mathbf{e} = \frac{\cos E - e}{1 - e\cos \mathrm{E}} \approx (\cos E - e)(1 + e\cos E) \approx \cos E - e\sin^2 E \tag{A43}$$

$$\sin\theta = \frac{\sqrt{1 - e^2}\,\sin E}{1 - e\cos \mathrm{E}} \approx \sin E(1 + \mathrm{e}\cos E) \tag{A44}$$

and their corresponding first-order inverses

$$\cos E \approx \cos\theta + e\sin^2\theta \tag{A45}$$

$$\sin E \approx \sin\theta(1 - e\cos\theta) \tag{A46}$$

arc used to convert to a single anomaly variable. The total change of $X \in \{e, \omega\}$ over an orbit is

$$\Delta X_{orb} = \int_{I \subset [0,2\pi]} \frac{dX}{d\varphi}\,d\varphi \tag{A47}$$

where φ is either angular variable (E or θ), and $dX/d\varphi$ *is* obtained by expressing equations A36 or A37 in terms of the chosen angular variable via the substitutions in equations A40 through A46 ' The interval of integration I is the range of angles over which the force is nonzero. Drag is always nonzero, hence the integral is taken over the entire range from O to 2π, whereas solar radiation pressure is only nonzero when the satellite is not in the Earth's shadow, and there is a smaller interval of integration. Finally, the long term variation in the element is approximated by the change over a single orbit divided by period,

$$\frac{dX}{dt} \approx \frac{n\Delta X_{orb}}{2\pi} \tag{A48}$$

Drag Perturbation on Eccentricity. The change in eccentricity due to drag over a single orbit for a satellite of mass m and constant area A normal to the direction of motion is given by Meirovitch[33]

$$\Delta e = -\frac{AaC_D\left(1 - \right.}{m}\int_0^{:\pi} \rho(E)\sqrt{\frac{1 + \mathrm{e}\cos E}{1 - e\cos E}}\cos E\,dE \tag{A49}$$

where $\rho(E)$ gives the density as a function of the eccentric anomaly and C_D is the coefficient of dreg. Keeping terms only to first order in e,

$$\frac{de}{dt}_{Drag} \approx \frac{nAe}{2\pi} \approx -\frac{K}{2\pi}\int_0^{2\pi} \rho(E)\left[1 + (e/2)\cos E + \cdots\right]^2 \cos E\,dE = -K(\rho_1 + ep2) \tag{A50}$$

where the orbital period is $P = 2\pi/n$, n *is the* mean motion, $K = naAC_D/m$, $p_l = (1/2\pi)\int_0^{2\pi}\rho(E)\cos E\,dE$, and $P2 = (1/2\pi)\int_0^{2\pi}\rho(E)\cos^2 E\,dE$.

Drag Perturbation on Argument of Perigee, To obtain an equation for the argument of perigee, wc start with Lagrange's planetary equation for de/dt and follow Meirovitch's method for obtaining equation A49. Meirovitch (equation 12.32) obtains the following result by inserting the drag force into Lagrange's planetary equations:

$$\frac{d\omega}{dt} = -\frac{A\rho v^2 C_D\left(1-e^2\right)\sin\theta}{mnae\sqrt{1+e^2+2e\cos\theta}} \approx -\frac{A\rho v^2 C_D\left(1-e^2\right)\sin\theta(1+e\cos\theta)}{mnae} \tag{A51}$$

where θ is the true anomaly, By applying basic formulae for elliptical motion, he also obtains an expression for the square of the velocity (equation 12.34):

$$v^2 = \frac{n^2a^2\left(1+e^2+2e\cos\theta\right)}{1-e^2} \approx n^2a^2(1+2e\cos\theta) \tag{A52}$$

Combining the last two results and expanding in terms of the small parameter e gives

$$\frac{d\omega}{dt} \approx -\frac{K}{e}\rho(\theta)\sin\theta(1+e\cos\theta) \tag{A53}$$

Combining the last several results and keeping terms to first order in e gives

$$\begin{aligned}\frac{d\omega}{dE} &= \frac{d\omega}{dt}\frac{dE}{dt} = -\frac{K}{ne}\sin\theta(1+e\cos\theta)(1-e\cos E)\\ &= -(K/ne)\sin E(1+e\cos E)(1+e\cos E)(1-e\cos E)\\ &\approx -(K/ne)\sin E(1+e\cos E)+\cdots\end{aligned} \tag{A54}$$

Then

$$\left.\frac{d\omega}{dt}\right|_{Drag} \approx \frac{n}{2\pi}\int_0^{2\pi}\frac{d\omega}{dE}dE = -\frac{K}{e}(\rho_3+\rho_4) = -\frac{K\rho_5}{e} \tag{A55}$$

where $\rho_5 = \rho_3 + p_4$, $\rho_3 = (1/2\pi)\int_0^{2\pi}\rho(E)\sin E dE$ and $\rho_4 = (1/2\pi)\int_0^{2\pi}\rho(E)\sin E\cos E dE$.

Along-Track Thrust Perturbation on Eccentricity. Assuming a continuos along-track thrust,

$$\Delta e_{orb} \cdot \frac{Av\cos O}{naa} \approx \frac{2T}{mn^2a}(\cos E - e)dE \tag{A56}$$

Letting $T=mdv/dt$ and making a circular orbit approximation ($v=na$, $\Delta v/v \approx As/2a$, $T \approx (mv/2a)da/dt$),

$$\frac{de}{dt} = \frac{n}{2\pi}\Delta e_{orb} \approx \frac{n}{2\pi}\frac{2T}{n^2am}\int_0^{2\pi}(\cos E - e)dE = \frac{-2T}{nam}e \approx -\frac{e}{a}\frac{da}{dt} \tag{A57}$$

Along-Track Thrust Perturbation on Argument of Perigee. A continuous along-track thrust has no affect upon the argument of perigee. Substituting equations A40 and A56 into A37,

$$\text{A m} = -\frac{F\left(1-e^2\right)}{mn^2ae^2}\sin E\left[\frac{1}{1-e\cos E}+\frac{1}{1-e^2}\right]dE \tag{A58}$$

which is an odd function in eccentric anomaly. Hence the integral over ar! orbit is zero.

Solar Radiation Pressure Perturbation on Eccentricity. The satellite is treated as a perfectly reflecting sphere, and hence the only momentum transfer is along the sun-satellite line. The geometry is illustrated in figure 11. The force can be expressed as[34] $F = SAC_R/c$, where A is the cross-sectional area normal to the sun line, c is the speed of light, S is the mean solar radiative flux at the earth, C_R is a constant which partially accounts for differences from sphericity and ideal reflection,

$$S \approx \frac{1358}{1.0004 + 0.0334\cos d}\ \text{W/m}^2 \tag{A59}$$

and d is the temporal phase angle measured in radians from July 4 (one year = 2π). Expressing the satellite to sun unit vector in terms of the angles β' (the declination of the sun above the plane of the satellite's

orbit) and α (measured in the plane of the orbit from perigee to the projection of the earth-sun line onto the satellite's orbit), the radial, along track and transverse components of the radiative force are*

$$F \approx \left(-F\cos\beta\cos(\theta - a),\quad F\cos\beta\sin(\theta-\alpha), F\ \sin\ \beta\right) \tag{A60}$$

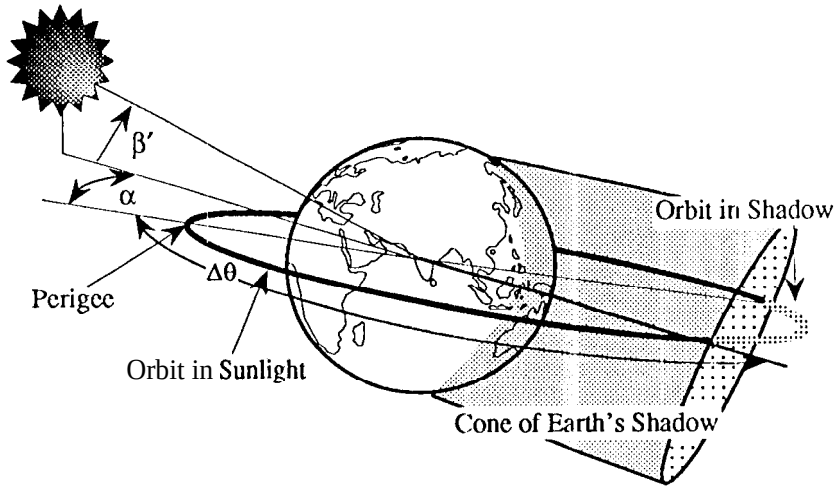

Figure 11. Geometry of solar radiation pressure perturbation.

Substituting equations A60 and A40 through A46 the change in eccentricity over an orbit is

$$\Delta e_{orb} = \frac{F\,COS\,\beta}{n^2} \int_{\alpha-\Delta\theta}^{\alpha+\Delta\theta} (1 - e\cos E)\left[2\cos\theta\sin(\theta-\alpha) - \sin\theta\cos(\theta-\alpha)\right] dE \tag{A61}$$

Differentiating equation A42 and applying equation A45, the variable of integration can be changed to O,

$$dE(1 - e\cos E) \approx d\theta(1 - 2e\cos O) \tag{A62}$$

Integrating equation A61 and only keeping terms to lowest order in e,

$$\frac{de}{dt} \approx \frac{n\Delta e_{orb}}{2\pi} \approx \frac{F\cos\beta'\sin\alpha}{2\pi ma n}\left\{-2\Delta\theta + \cos\alpha\ \sin\ \Delta\theta\left[1 + 4\cos\alpha\cos\Delta\theta\right]\right\} \equiv H(\alpha, \beta') \tag{A63}$$

where the entire right hand side has been lumped into the function $H(\alpha,\beta')$ to highlight the explicit independence of de/dt from either e or ω. The shadow entrance and exit angles arc given by Escobal as a quartic in $\cos\theta$. For a circular orbit the solution reduces to a quadratic, and

$$\Delta\theta \approx \pi - \cos^{-1}\left\{\left[1 - (R_e/a)^2\right]^{1/2} / \cos\beta'\right\} \tag{A64}$$

Solar Radiation Pressure Perturbation on Argument of Perigee. Substituting equations A60 and A60 into A39 and keeping only terms to the lowest order in e, the orbital change in ω is

$$\Delta\omega_{orb} = \frac{-F}{maen^2} \int_{\alpha-\Delta\theta}^{\alpha+\Delta\theta} \left[-\cos\beta'\cos(\theta-\alpha)\cos\theta + 2\cos\beta'\sin(\theta-\alpha)\sin\theta\right] d\theta \tag{A65}$$

Expanding the trigonometric functions in equation A65,

$$\begin{aligned}\Delta\omega_{orb} = \frac{-F}{maen^2}\Big\{ & -\cos\beta'\cos\alpha \int_{\alpha-\Delta\theta}^{\alpha+\Delta\theta} \cos^2\theta\, d\theta \ \text{-cms~'sins} \int_{\alpha-\Delta\theta}^{\alpha+\Delta\theta} \cos\theta\sin\theta\, d\theta d\theta \\ & + 2\cos\beta'\cos a \int_{\alpha-\Delta\theta}^{\alpha+\Delta\theta} \sin^2\theta\, d\theta \ - \ 2\text{cosp'sins} \int_{\alpha-\Delta\theta}^{\alpha+\Delta\theta} \sin\theta\cos\theta\, d\theta \quad 1\end{aligned} \tag{A66}$$

* Ignoring variations due to the satellite orbit itself, which $\approx a^2/R^2$ when R is the earth to sun distance.

The integrals in equation A66 can be evaluated by observing that

$$\int_{\alpha-\Delta\theta}^{\alpha+\Delta\theta} \cos^2\theta d\theta = \Delta\theta + \frac{1}{2}\cos 2\alpha \sin 2\Delta\theta \tag{A67}$$

$$\int_{\alpha-\Delta\theta}^{\alpha+\Delta\theta} \cos\theta \sin\theta d\theta = \frac{1}{2}\sin\ 2\text{asin2A0} \tag{A68}$$

$$\int_{\alpha-\Delta\theta}^{\alpha+\Delta\theta} \sin^2\theta d\theta = \Delta\theta - \frac{1}{2}\cos 2\alpha \sin 2\Delta\theta \tag{A69}$$

The long term perturbation one is then

$$\frac{d\omega}{dt} \approx \frac{n\Delta\omega_{orb}}{2\pi r} \frac{-F\cos\beta'\cos\frac{a}{}}{2\pi mae} \left[\Delta\theta - \frac{3}{2}\sin(2\Delta\theta)\right] \equiv \frac{W(a,\beta')}{e} \tag{A70}$$

where the geometric variables have been grouped into the function $W(\alpha,\beta')$.

REFERENCES

1. Cutting, E., G. H. Born, and J. C. Frautnick, "Orbit Analysis for SEASAT-A, " *Journal of the Astronautical Sciences,* Vol. XXVI, Oct.-Dee. 1978 pp. 315-342.9.
2. Herder, R. W., M. F. Cullen, and A. B. Glass, *Description and Application of the Frozen Orbit Concept,* CSC/TP-79/6089, Computer Sciences Corporation, 1979.
3. Nickerson, K. G., R. W. Herder, A. B. Glass, and J. L. Cooley, "Application of Altitude Control Techniques for Low Altitude Earth Satellites," *Journal of the Astronautical Sciences,* Vol. XXVI, Apr. - Jun. 1978, pp. 129-148.
4. McIntosh, J. R. and P. J. Hassett, *Landsat-4 Orbit Adjust Maneuver Report, CSC-TP-82-6232,* Computer Sciences Corporation, 1982.
5. Born, George H., Jim L. Mitchell, "GEOSAT ERM Mission Design, " *Journal of the Astronautical Sciences,* Vol. 35, Apr. -Jun. 1987, pp. 119-134.
6. Born, George H., Patrick Allen, Charles Kilgus, and Antonino Pino, "Orbit Analysis for the GEOSAT ERM," *Journal of the Astronautic/ Sciences,* Vol. 36, Oct. - Dec. 1988, pp. 425-446.
7. Shapiro, Bruce, "The GEOSAT Orbit Adjust," *Journal of the Astronautical Sciences,* Vol. *36,* Oct.-Dee. 1988, pp. 407-424.
8. Shapiro, Bruce and Antonino Pino, "Maintenance of An Exact Repeat Ground Track - The GEOSAT ERM," AIAA/AAS Astrodynamics Conference, Minneapolis, Minnesota, Aug. 1988.
9. Smith, J. C., "Analysis and Application of Frozen Orbits for the TOPEX Mission," AIAA Paper 86-2069 - CP, AIAA/AAS Astrodynamics Conference, Williamsburg, Virginia, Aug. 1986.
10. Vincent, Mark, "Eccentricity and Argument of Perigee Control for Orbits with Repeat Ground Tracks," Paper AAS-91 -516, AAS/AIAA Astrodynamics Specialists Conference, Durango, Colorado, Aug. 1991.
11. Foister, James W., III, "Frozen Orbit Analysis in the Martian System," M.S. Thesis, Air Force Institute of Technology, Dec. 1987.
12. Rosborough, George and Cesar A. Ocampo, "Influence of Higher Degree Zonals on the Frozen Orbit Geometry," Paper AAS 91-428, AAS/AIAA Astrodynamics Conference, Durango, Colorado, Aug. 1991.
13. Uphoff, C, "Frozen Polar Lunar Orbits," Jet Propulsion Laboratory IOM 312/76.3-2, 1976 (Internal Document).
14. Uphoff, C. and P. H. Roberts, "Orbit Design Concepts for Venus Orbiter," Paper AAS-78-1437, AAS/AIAA Astrodynamics Conference, Palo Alto, CA, Aug. 1978.
15. Murrow, Richard C., *Frozen Orbits - Near Constant or Beneficially Varying Orbital Parameters,* Univ. Of Colorado, Ph.D. Dissertation, 1986.
16. Chobotov, Vladimir A., *Orbital Mechanics,* Washington, DC: American Institute of Aeronautics and Astronautics, 1991.
17. Coffey, S, A. Deprit, and E. Deprit, "Painting Phase Spaces to Put Frozen Orbits in Context," Paper AAS 91-427, AAS/AIAA Astrodynamics Specialist Conference, Durango, Colorado, Aug. 1991.

18. Coffey, Shannon L., Andre Deprit, and Etienne Deprit, "Frozen Orbits Close lo an Earth-like Planet, " *Celestial Mechanics and Dynamical Astronomy, vol.* 59, pp. 37-72, 1994.

19. Guckenheimer, John and Philip Holmes, *Nonlinear Oscillations, Dynamical Systems, and Bifurcations of Vector fields, New* York: Spring er-Verlag, 1986.

20, Bhat, Ramachandra, Bruce E. Shapiro and Raymond B. Frauenholz, "TOPEX/Poseidon Orbit Acquisition Maneuver Sequence," Paper AAS 93-571, AAS/AIAA Astrodynamics Specialist Conference, Victoria, B. C., Canada, Aug. 1993.

21. Merson, R. H., 'The Dynamic Model of PROP, A Computer Program for the Refinement of the Orbital Parameters on an Earth Satellite," RAE-TR-66255, Royal Aircraft Establishment, Farnborough Hants, England, 1965.

22. Groves, G. V., "Motion of a Satellite in the Earth's Gravitational Field," *Proc. Roy. Sot.,* vol. *254,* pp. *48-65,* 1960.

23. Coffey, Shannon L., Andre Deprit, and Bruce R. Miller, 'The Critical Inclination in Artificial Satellite Theory," *Celestial Mechanics,* vol. *39,* **pp. 365-406, 1986.**

24. Roberts, Charles, "An Analytic Model for Upper Atmosphere Densities Based Upon Jacchia's 1970 Models," *Celestial Mechanics,* Vol. *4,* pp. 368-377, 1971.

25. Long, A. C., J. O. Cappellari, C. E. Velez, and A. J. Fuchs, *Goddard Trajectory Determination System (GTDS) Mathematical Theory, Revision 1,* NASA/GSFC Flight Mechanics Division, FDD/552-89/001, July 1989.

26. Frauenholz, Ray, Tom Hamilton, Bruce Shapiro and Ram Bhat, "The Role of Anomalous Satellite Fixed Accelerations in TOPEX/Poseidon Orbit Maintenance," Paper AAS-93-57O, AAS/AIAA Astrodynamics Specialist Conference, Victoria, B. C., Canada, Aug. 1993.

27. Richter, Robert, "Determination of Satellite Acceleration," Jet Propulsion Laboratory 10M-3544-TOP-93-004, Sept. 1, 1993 (Internal Document).

28. Richter, Robert, "Radiation Forces Acting on the TOPEX/Poseidon Spacecraft Along the Velocity Vector due to the Solar Array - Initial Results," Jet Propulsion Laboratory IOM 3544-TOP-93-3, Jul. 8, 1993 (Internal Document).

28. Shapiro, Bruce and Ram Bhat, "GTARG - The TOPEX/Poseidon Ground Track Maintenance Maneuver Targeting Program," Paper AIAA 93-1129, AIAA Aerospace Design Conference, Irvine, CA, Feb. 1993.

29. Doll, C. E., D. H. Oza, J. M. Loran, and D. T. Bolvin, "Accurate Orbit Determination Strategies for TOPEX/Poseidon Using TDRSS," AIAA Guidance, Navigation, and Control Conference, Baltimore, MD, Aug. 1995.

30. Guinn, J. R., "Short Period Gravitational Perturbations for Conversion Between Osculating and Mean Orbit Elements," Paper AAS 91-430, AAS/AIAA Astrodynamics Specialists Conference, Durango, CO, Aug. 1991.

31. Frauenholz, R. B., R. S. Bhat, B. E. Shapiro and R. K. Leavitt, "An Analysis of the TOPEX/Poseidon Operational Orbit: Observed Variations and Why," Paper AAS-95-366, AAS/AIAA Astrodynamics Specialists Conference, Halifax, Nova Scotia, Canada, Aug. 1995.

32. Arfken, George, *Mathematical Methods for Physicists,* Second Edition, New York: Academic, 1970.

33, Meirovitch, Leonard, *Methods of Analytical Dynamics, New* York: McGraw Hill, 1970.

34. Wertz, J. R., *Spacecraft Attitude Determination and Control,* Boston: Reidel, 1978.

35. Escobal, Pedro Ramon, *Methods of Orbit Determination,* Malabar, Florida: Krieger, 1965.

36. Shapiro, Bruce, "Computing Satellite Maneuvers for a Repeating Ground Track, " *NASA Tech Briefs, Vol 18, No. 12,* pp. 60-61, Dec. 1994.